J. Solid Mech. 2025; 17(04): Article 16

Journal of Solid Mechanics

https://doi.org/10.57647/jsm.2025.1704.16

Research Article

Buckling Analysis of Functionally Graded Materials of Thin Rectangular Plates Applying the Modified Differential Quadrature Method

Reza Kazemi[1], Mohsen Rafiei Karahroudi[2], Seyed Alireza Mousavi Shirazi[3,*]

[1]*Department of Mechanical Engineering, Arak.C., Islamic AZAD University, Arak, Iran*
[2]*Department of Nuclear Engineering, SR.C., Islamic AZAD University, Tehran, Iran*
[3]*Department of Physics, ST.C., Islamic AZAD University, Tehran, Iran*

***Corresponding author:** alireza.mousavishirazi@iau.ac.ir

Article History:

Received:
03 September 2025

Revised:
05 December 2025

Accepted:
11 December 2025

Published in Issue:
31 December 2025

Abstract

This study investigates the buckling behavior of thin rectangular plates composed of Functionally Graded Materials (FGMs) using the Modified Differential Quadrature Method (MDQM). Through the application of this method, the governing differential equations are transformed into a system of linear algebraic equations suitable for buckling analysis. After defining the relevant parameters, the problem formulation enables the computation of buckling coefficients. The buckling response of the plates under compressive loading is examined for various boundary conditions, and the influence of fixed boundary effects on the resulting buckling coefficients is analyzed. The results obtained using the MDQM are compared with corresponding analytical solutions and finite element analysis outcomes. The comparisons demonstrate that the proposed approach effectively predicts the buckling loads of rectangular plates under different boundary conditions. It is also observed that the accuracy of the results is highly sensitive to the number of grid points employed; insufficient grid density leads to non-convergent solutions, indicating that careful discretization is essential for reliable application of the MDQM. Furthermore, the buckling coefficient is shown to vary significantly with boundary conditions. Overall, the close agreement between MDQM results and finite element data confirms the suitability of the method for analyzing the buckling behavior of non-uniform plates.

Keywords: Buckling Analysis; Compressive Load; Functionally Graded Materials; MDQM

Cite this article: Kazemi, R., Rafiei Karahroudi, M., Mousavi Shirazi, S. A., (2025). Buckling Analysis of Functionally Graded Materials of Thin Rectangular Plates Applying the Modified Differential Quadrature Method, *Journal of Solid Mechanics,* 17(04): Article 16.
https://doi.org/10.57647/Jsm.2025.1704.16

1. Introduction

In recent years, the majority of studies on buckling phenomena have focused on structures composed of homogeneous materials, predominantly isotropic ones [1]. Extensive research has been devoted to the buckling behavior of beams, plates, rings, cylindrical shells, and general shell structures made of homogeneous and isotropic materials subjected to mechanical loading conditions [2,3].

Moreover, buckling analyses have been performed on various plate types under mechanical and thermal loads based on first-order and higher-order shear deformation theories [4,5].

A key aspect in buckling analysis is the numerical or analytical method employed to solve the governing equations. One such method is the Differential Quadrature Method (DQM) [6, 7], which has gained considerable attention in recent years due to its high efficiency in solving partial differential equations associated with linear and nonlinear boundary value problems [8, 9]. The DQM is based on approximating partial derivatives of a function at discrete points through weighted linear summations of function values [10]. In the present study, the MDQM is employed to determine the buckling coefficients of rectangular plates made of Functionally Graded Materials (FGMs) subjected to non-uniform linear edge loading [11, 12].

A major challenge in this context lies in accurately determining the in-plane stress distribution within the plate, which constitutes a crucial preliminary step in buckling analysis. This issue has been addressed in previous studies, where density variation along a single axis following a half-sine distribution was investigated [13]. Subsequently, parabolic density distributions were examined, and an energy-based formulation was introduced to improve solution accuracy [14, 15]. In the framework of the DQM, since the grid-point values of the unknown function are treated as independent variables, the direct imposition of boundary conditions particularly for higher-order derivatives can lead to computational difficulties, such as those encountered when solving fourth-order differential equations [16]. To overcome these limitations, alternative strategies have been proposed [17] in which boundary conditions associated with higher-order derivatives are transformed into equivalent linear equations using appropriate weighting coefficients, thereby enabling the consistent enforcement of all boundary conditions [18]. It has also been reported that, when applying the DQM to buckling problems of rectangular plates under uniform edge loading, the numerical results exhibit a high sensitivity to the number and distribution of grid points [19] . To alleviate this sensitivity, modified approaches incorporating non-uniform grid distributions have been developed [20–22], which have demonstrated improved performance in the analysis of buckling behavior in non-homogeneous plates [23].

In contrast to conventional formulations based on second-order partial differential equations, the DQM formulation adopted in this study employs a fourth-order partial differential equation expressed in terms of the Airy stress function [24]. This approach allows for the accurate determination of stress distributions under non-uniform in-plane loading. However, its applicability has generally been limited to cases involving linear or uniformly distributed loads [25,26]. The present article extends this framework to evaluate improved buckling coefficients for FGM rectangular plates subjected to parabolic in-plane compressive loading and compares the resulting predictions with those obtained using the Finite Element Method (FEM) [27, 28].

2. Materials and methods

In recent years, FGMs have gained increasing attention in industrial applications, particularly in high-temperature environments such as nuclear reactors. Owing to their unique structural characteristics, the performance and applicability of FGMs are expected to further expand in the coming years. FGMs are engineered composite materials with a refined microstructure and inherent non-homogeneity, in which mechanical properties vary gradually and continuously across the material thickness. This behavior is achieved through a controlled and progressive variation in the volume fractions of the constituent materials. FGMs are most commonly fabricated by combining ceramic and metallic phases. For instance, in a cubic sample, the top surface may consist entirely of ceramic, while the bottom surface is composed of pure metal. The intermediate region comprises a gradual mixture of ceramic and metal constituents, as schematically illustrated in Figure 1.

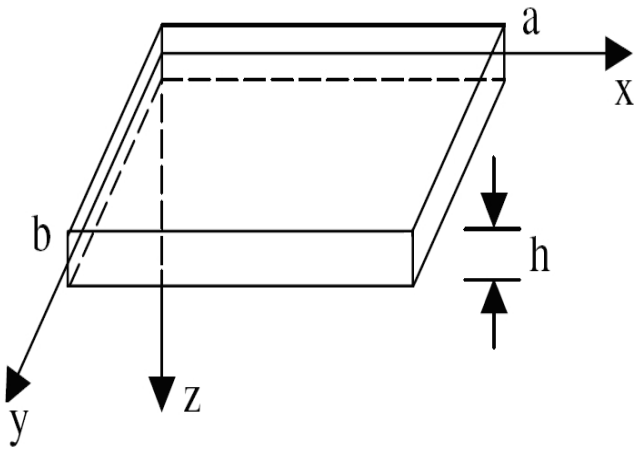

Figure 1. Specifications of the system and geometric features of a rectangular plate

The effective modulus of elasticity (E) and the coefficient of thermal expansion (α) are defined as follows [29]:

$$E(z) = E_c V_c + E_m(1 - V_c)$$

$$\alpha(z) = \alpha_c V_c + \alpha_m(1 - V_c) \quad (1)$$

$$\nu(z) = \nu_\circ$$

In these expressions, the subscripts m and c denote the properties of the metal and ceramic phases, respectively.

10.57647/Jsm.2025.1704.16

The volume fraction of ceramic to metal ($\frac{V_c}{V_m}$), based on the power-law distribution, is expressed as:

$$V_c = (\frac{2z+h}{2h})^p$$
$$V_m = 1 - V_c \quad (2)$$

In this formulation, the coordinate z represents the variation through the plate thickness ($-\frac{h}{2} \le z \le \frac{h}{2}$). The thickness and P denote the power-law indices ($P \ge 0$). Additional material properties of the FGM plate are defined according to the relations proposed by Reddy [30]:

$$E(z) = E_m + E_{cm}(\frac{2z+h}{2h})^p$$
$$\alpha(z) = \alpha_m + \alpha_{cm}(\frac{2z+h}{2h})^p \quad (3)$$
$$\nu(z) = \nu_\circ$$

Where E_{cm} and α_{cm} are given by:

$$E_{cm} = E_c - E_m$$
$$\alpha_{cm} = \alpha_c - \alpha_m \quad (4)$$
$$(E_1, E_2, E_3) = \int_{-h/2}^{h/2} (1, z, z^2) E(z) dz$$

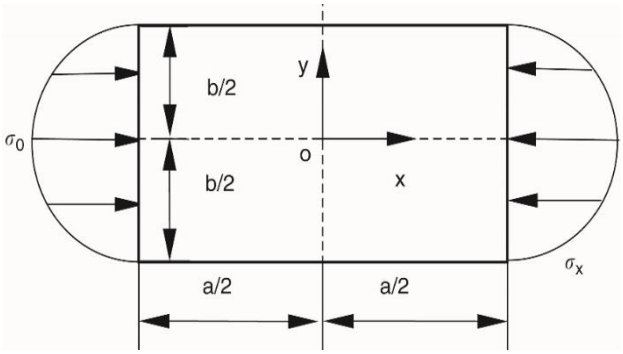

Figure 2. Rectangular plate subjected to nonlinear cosine compressive loading

Figure 1 illustrates the representative FGM specimen in the form of a cube.

2.1. Governing differential equations

In this section, the elasticity problem of a rectangular FGM plate with length a and width b, subjected to edge loading, is examined.

A schematic representation of the rectangular plate is shown in Figure 2.

Since the boundary conditions of the present problem are stress-based, stress-function approaches are employed to determine the stress distribution within the plate. Accordingly, the Airy stress function (Q) is introduced to satisfy the prescribed boundary conditions.

The governing Airy stress equations, which are independent of the volume fraction distribution, are expressed as follows:

$$\sigma_x = \frac{\partial^2 Q}{\partial y^2}, \sigma_y = \frac{\partial^2 Q}{\partial x^2}, \tau_{xy} = -\frac{\partial^2 Q}{\partial x \partial y} \quad (5)$$

The Airy stress function must also satisfy the following compatibility equation:

$$\frac{\partial^4 Q}{\partial x^4} + 2\frac{\partial^4 Q}{\partial x^2 \partial y^2} + \frac{\partial^4 Q}{\partial y^4} = 0 \quad (6)$$

By solving Eq. 6, the Airy stress function Q can be determined. Substituting the obtained expression for Q into Eq. 5 yields the corresponding Airy stress components.

To compute the numerical values of Q, the Discrete Quadrature (DQ) method is employed in conjunction with approximate boundary conditions. It should be noted that stress boundary conditions cannot be imposed directly within the DQ framework.

Therefore, to evaluate the values of the Airy stress function at discrete grid points over the rectangular plate, the discretization scheme illustrated in Figure 3 is adopted.

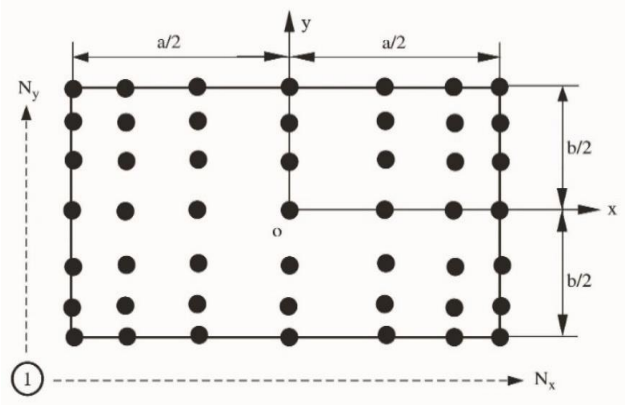

Figure 3. Grid point distribution over the rectangular plate

$$a)\ (Q_y)_B = (\frac{\partial Q}{\partial y})_B = \int_A^B \sigma_x ds = \int_A^B \overline{X} ds$$
$$b)\ (Q_x)_B = (\frac{\partial Q}{\partial x})_B = \int_A^B \sigma_y ds = -\int_A^B \overline{Y} ds \quad (7)$$
$$c)\ Q_B = \int_A^B (y_B - y)\overline{X} ds - \int_A^B (x_B - x)\overline{Y} ds$$

In Eq. 7, $\overline{X}$ and $\overline{Y}$denote the in-plane load components applied at the boundary in the x- and y-directions, respectively.
Points A and B represent specific locations along the boundary; point A corresponds to point 1 in Figure 3, while point B is selected depending on the edge over which the integration is performed. Initially, the following assumption is made:

$$Q_A = (\frac{\partial Q}{\partial x})_A = (\frac{\partial Q}{\partial y})_A = 0 \tag{8}$$

To derive Eq. 7, the following operation is applied:

$$\sigma_x = \frac{\partial^2 Q}{\partial y^2} \tag{9}$$

Integrating both sides of the resulting expression with respect to y yields:

$$\int_A^B \sigma_x dy = \int_A^B \frac{\partial^2 Q}{\partial y^2} dy = \frac{\partial Q}{\partial y}) \Big| \begin{matrix} B \\ A \end{matrix} = \frac{\partial Q}{\partial y})_B - \frac{\partial Q}{\partial y})_A$$
$$\xrightarrow{(8)} \frac{\partial Q}{\partial y})_B = (Q_y)_B = \int_A^B \sigma_x dy = \int_A^B \overline{X} ds \tag{10}$$

Thus, to demonstrate Eq. 7b, a similar procedure is followed, leading to:

$$\sigma_y = \frac{\partial^2 Q}{\partial x^2} \tag{11}$$

Integrating both sides of Eq. 11 with respect to x yields:

$$(\frac{\partial Q}{\partial x})_B = (Q_x)_B = \int_A^B \sigma_y dx = -\int_A^B \overline{Y} ds \tag{12}$$

Next, Eq. 7c is derived. By differentiating the function $Q(x,y)$, the following expression is obtained:

$$dQ = \frac{\partial Q}{\partial x} dx + \frac{\partial Q}{\partial y} dy \tag{13}$$

Integrating both sides of this equation results in:

$$\int_A^B dQ = \int_A^B \frac{\partial Q}{\partial x} dx + \int_A^B \frac{\partial Q}{\partial y} dy$$
$$Q_B - Q_A = \int_A^B \int_A^B \overline{X} ds dy - \int_A^B \int_A^B \overline{Y} ds dx$$
$$= \int_A^B \overline{X} (\int_A^B dy) ds - \int_A^B \overline{Y} (\int_A^B dx) ds \tag{14}$$
$$Q_B = \int_A^B (y_B - y)\overline{X} ds - \int_A^B (x_B - x)\overline{Y} ds$$

Accordingly, the Airy stress functions at the boundary for specific loading conditions can be expressed as follows:

$$\overline{X}(x = \frac{a}{2}) = \frac{4\sigma_0}{b^{(2)}}(y^2 - \frac{b^2}{4})$$
$$\overline{X}(x = -\frac{a}{2}) = -\frac{4\sigma_0}{b^{(2)}}(y^2 - \frac{b^2}{4}) \tag{15}$$

The stress functions along the boundaries $y = \pm\frac{b}{2}$ are evaluated under the assumption of $Q_i = (\frac{\partial Q}{\partial y})_i = 0$:

$$y = -\frac{b}{2}$$
$$Q_i = \int_{-b/2}^{b/2} (y_B - y)\overline{X} ds = 0 \tag{16a}$$
$$Q_y = \int_{-b/2}^{b/2} \overline{X} ds = 0$$

$$y = \frac{b}{2}$$
$$Q_i = \int_{-b/2}^{y_i} (\frac{b}{2} - y)\frac{4\sigma_0}{b^2}(y^2 - \frac{b^2}{4}) dy \tag{16b}$$
$$\rightarrow Q_i = -\frac{\sigma_0 b^2}{3}$$

To determine the stress functions along the remaining boundaries $x = \pm\frac{a}{2}$, the same procedure is followed under the assumption $(Q_x)_i = 0$:

$$Q_i = \int_{-b/2}^{y_i} (y_i - y)\frac{4\sigma_0}{b^2}(y^2 - \frac{b^2}{4}) dy$$
$$Q_i = \frac{\sigma_0}{48b^2}[16y_i^4 - 24b^2 y_i^2 - 16b^3 y_i - 3b^4] \tag{17}$$

This procedure yields the corresponding stress functions for the prescribed loading conditions:

$$X = \sigma_x = \sigma_\circ cos(\frac{\pi y}{b})$$
$$\sigma_y = \tau_{xy} = 0 \tag{18}$$

$$x = \pm\frac{a}{2}, (Q_x)_i = 0$$
$$Q_i = \frac{\sigma_\circ b}{\pi}[-\frac{b}{\pi}cos(\frac{\pi y_i}{b}) + y_i + \frac{b}{2}] \tag{19a}$$

10.57647/Jsm.2025.1704.16

$$y=\frac{b}{2}\rightarrow (Q_y)_i=\frac{2\sigma_\circ b}{\pi}, Q_i=\frac{\sigma_\circ b^2}{\pi}$$
$$y=-\frac{b}{2}\rightarrow Q_i=(Q_y)_i=0 \quad (19b)$$

The buckling behavior of the FGM rectangular plate illustrated in Figure 2 is now examined. The governing differential equation for buckling under in-plane loading is given by:

$$\frac{E_2^2-E_1E_3}{E_1(1-\nu_\circ{}^2)}\nabla^4 w_1+N_{x\circ}w_{1,xx}+N_{y\circ}w_{1,yy}+2N_{xy\circ}w_{1,xy}=0 \quad (20)$$

In this equation, $N_{x\circ}, N_{y\circ}, N_{xy\circ}$ represent the pre-buckling forces obtained from the solutions of the corresponding equilibrium equations. By expressing these forces in terms of the associated stress components, Eq. 20 can be rewritten as:

$$D\nabla^4 w=\sigma_x h\frac{\partial^2 w}{\partial x^2}+2\sigma_{xy}h\frac{\partial^2 w}{\partial x\partial y}+\sigma_y h\frac{\partial^2 w}{\partial y^2} \quad (21)$$

Where D denotes the flexural rigidity of the FGM plate:

$$D=\frac{E_2^2-E_1E_3}{E_1(1-\nu_\circ{}^2)} \quad (22)$$

In this formulation, h represents the plate thickness, w denotes the transverse deflection, and the in-plane stress components $\sigma_x, \sigma_y, \tau_{xy}$ are calculated using Eq. 5. The bending moment is defined as:

$$M_x=-D\left(\frac{\partial^2 w}{\partial x^2}+\mu\frac{\partial^2 w}{\partial y^2}\right)$$
$$M_y=-D\left(\mu\frac{\partial^2 w}{\partial x^2}+\frac{\partial^2 w}{\partial y^2}\right) \quad (23)$$

2.2. Boundary conditions

1. Simply Supported Base:

$$x=-\frac{a}{2},\frac{a}{2}\rightarrow w=M_x=0$$
$$y=-\frac{b}{2},\frac{b}{2}\rightarrow w=M_y=0 \quad (24)$$

2. Clamped Base:

$$x=-\frac{a}{2},\frac{a}{2}\rightarrow w=w_x=0$$
$$y=-\frac{b}{2},\frac{b}{2}\rightarrow w=w_y=0 \quad (25)$$

2.3. Modified differential quadrature method (MDQM)

The Differential Quadrature Method (DQM) is a simple yet efficient numerical technique for solving both linear and nonlinear partial differential equations, particularly those arising in boundary value problems. However, due to certain limitations associated with the conventional formulation, the method has been extended and refined to overcome these challenges. In this section, the MDQM is briefly reviewed.

In the standard DQM, the approximation of the s-th derivative of the solution function at grid point i is expressed as:

$$Q_i^{(S)}=\sum_{j=1}^{n}E_{ij}^{(S)}Q_j, i=1,2,\ldots,n \quad (26)$$

Where $E_{ij}^{(S)}$ denotes the weighting coefficient corresponding to the s-th derivative of the solution function at grid points i and j [31]. The parameter n represents the total number of grid points, including the boundary nodes, and Q_i denotes the value of the solution function at grid point j. The $E_{ij}^{(4)}, E_{ij}^{(3)}, E_{ij}^{(2)}$, and $E_{ij}^{(1)}$, weighting coefficients for the first, second, third, and fourth-order derivatives in the conventional DQM, are determined such that they accurately approximate the corresponding derivatives of the function $(i=1,2,\ldots,n; j=1,2,\ldots n)$.

The MDQM differs slightly from the classical formulation. The principal distinction lies in the introduction of the first derivative of Q at the two boundary points, $Q_n^{(1)}, Q_1^{(1)}$ as additional independent variables, which enhances the flexibility and accuracy of the method when enforcing boundary conditions:

$$\{u\}^T=\{Q_1,Q_2,\ldots,Q_{n-1},Q_n,Q_1^{(1)},Q_n^{(1)}\} \quad (27)$$

The weighting coefficients for the first-, second-, third-, and fourth-order derivatives in the MDQM are computed as follows [32, 33]:

$$A_{ij}=C_{ij}^{(1)}(i,j=1,2,\ldots,n)$$
$$A_{ij}=0(i=1,2,\ldots,n; j=n+1,n+2) \quad (28a)$$

$$B_{ij}=C_{ij}^{(2)}(i,j=1,2,\ldots,n)$$
$$B_{ij}=0(i=1,2,\ldots,n; j=n+1,n+2) \quad (28b)$$

The weighting coefficients associated with the third- and fourth-order derivatives are obtained using alternative formulations [34]. Accordingly, the expressions for the second- to fourth-order derivatives of the solution function are given as:

$$Q_i^{(2)} = \sum_{j=1}^{n+2} B_{ij} u_j$$
$$Q_i^{(3)} = \sum_{j=1}^{n+2} C_{ij} u_j \quad (29)$$
$$Q_i^{(4)} = \sum_{j=1}^{n+2} D_{ij} u_j \ , \ (i = 2,3,\dots,n-1)$$

To provide a clear justification and facilitate a more systematic presentation, the solution procedure is organized into five stages, as outlined below.

1. First Stage – Formulation of the Buckling Equation and Definition of the Critical Load Coefficient:

Based on Classical Plate Theory (CPT) and utilizing the derived stress results, the equilibrium equation of the plate at the onset of buckling can be expressed as follows [35]:

$$D\nabla^4 w = N_x \frac{\partial^2 w}{\partial x^2} + 2N_{xy} \frac{\partial^2 w}{\partial x \partial y} + N_y \frac{\partial^2 w}{\partial y^2} \quad (30)$$

Where $w\ (x, y)$ denotes the transverse deflection of the plate, and D represents the equivalent bending stiffness, which is a function of the material gradient properties of the FGM. The terms N_x, N_y, and N_{xy} correspond to the pre-buckling internal force components obtained from the Airy stress function. The primary objective is to determine the minimum scaling coefficient, or critical buckling load (λ), such that the governing equation admits a nontrivial solution. To this end, the internal force components are reformulated in normalized form of $N_x = \widehat{N}_x \lambda$, and the problem is cast as a linear eigenvalue problem. After extracting the initial stress field from the Airy stress function, the in-plane stability of the plate is analyzed. At this stage, the differential equation governing buckling is transformed into an eigenvalue problem and solved numerically using the MDQM.

2. Second Stage – Discretization of the Domain and Definition of Degrees of Freedom [36]:

The rectangular plate domain is discretized using a grid of $n_x \times n_y$ discrete points. In the modified MDQM, the degrees of freedom depend on the location and type of each grid point. At the corner points, three unknowns are defined, consisting of the transverse deflection w and the two slope components (w_x, w_y).

At boundary points along edges parallel to the x- and y-axes, four unknowns (w, w_x) and (w, w_y) are considered, respectively.

At interior grid points, only the transverse deflection w is treated as an unknown. Unlike the classical DQM, this formulation treats boundary derivatives as independent variables, which enables more accurate enforcement of geometric boundary conditions such as simply supported and clamped edges [37].

3. Third Stage – Approximation of Derivatives Using MDQM Weighting Coefficients:

The partial derivatives appearing in the governing equation (such as $\frac{\partial^4 w}{\partial x^4}$ or $\frac{\partial^2 w}{\partial x \partial y}$) at each grid point are approximated as linear combinations of the corresponding degrees of freedom. The coefficients of these linear combinations are the quadrature weighting factors, which are derived from interpolating polynomials such as Legendre or Chebyshev polynomials [38]. As an illustrative example, the fourth-order derivative of w with respect to the x-direction at the i-th grid point is expressed as:

$$\frac{\partial^4 w}{\partial x^4} | i \approx \sum_{j=1}^{N_x+2} D_{ij}^x u_j \quad (31)$$

Where u_j denotes the global vector of degrees of freedom, consisting of the transverse deflections w and the corresponding boundary derivatives. The coefficients D_{ij}^x represent the fourth-order derivative weighting factors in the MDQM. This approximation procedure is applied consistently to all required derivatives at each interior grid point.

4. Fourth Stage – Formation of the Eigenvalue Equation System:

In this stage, the MDQM approximations obtained in the previous step are substituted into both the governing buckling differential equation and the associated boundary condition equations. By enforcing these equations simultaneously on the unknown degrees of w, w_x, and w_y, an integrated system of linear algebraic equations is constructed. This system can be expressed in the following compact matrix form:

$$[K - \lambda G]U = 0 \quad (32)$$

Where U is the column vector containing all unknown variables (transverse deflections and slopes) defined over the computational grid; K is the plate bending stiffness matrix, obtained from the discretization of the differential operator and the imposition of static boundary conditions such as simply supported edges; G is the geometric stiffness matrix (also referred to as the initial stress matrix), derived from the discretization of the right-hand side of equation (N_x, N_y, N_{xy}); λ is the eigenvalue of interest, corresponding to the scaling factor of the critical buckling load.

5. Fifth Stage – Solution of the Eigenvalue Problem and Extraction of Results:

The resulting system of Eq. 32 constitutes a generalized eigenvalue problem. The smallest positive eigenvalue of this system corresponds to the critical buckling load of the plate (λ_{cr}). The associated eigenvector represents the corresponding buckling mode

10.57647/Jsm.2025.1704.16

shape [*w (x, y)*] [39]. These eigenvalue problems are typically solved using numerical software packages, such as MATLAB.

Finally, the commonly used dimensionless buckling coefficient (K) is calculated using the following relation:

$$K = \frac{\lambda_{cr} b^2}{\pi^2 D} \tag{33}$$

The results are presented for various parameters, including plate dimensions, material gradient, and boundary conditions.

One of the main advantages of the MDQM is that, through appropriate grid selection, fast and accurate convergence can be achieved.

2.4. Equations in the form of the MDQM

Referring to Figure 3, the total number of grid points (n_x, n_y) is distributed along the x- and y-directions. Both governing equations, Eqs. 6 and 21, are fourth-order partial differential equations. The MDQM is applied to discretize these equations.

At each corner grid point, three degrees of freedom are defined Q_y, Q_x, Q or w_y, w_x, w.

$$Q_y = \frac{\partial Q}{\partial y}, Q_x = \frac{\partial Q}{\partial x}$$
$$w_y = \frac{\partial w}{\partial y}, w_x = \frac{\partial w}{\partial x} \tag{34}$$

At the remaining boundary points, two degrees of freedom are considered.

For points located along edges parallel to the y-axis, the degrees of freedom are defined as Q_x, Q or w_x, w whereas for points along edges parallel to the x-axis, they are defined as Q_y, Q or w_y, w. Each interior grid point possesses only one degree of freedom, namely the transverse deflection w [40].

Within the DQM framework, the governing differential Eqs. 6 and 21 are discretized and expressed as follows:

$$\sum_{k=1}^{n_x} D_{ik}^x Q_{kl} + 2\sum_{j=1}^{n_x}\sum_{k=1}^{n_y} B_{ij}^x B_{lk}^y Q_{jk} + \sum_{k=1}^{n_y} D_{lk}^y Q_{ik}$$
$$+D_{i(n_x+1)}^x (Q_x)_{1l} + D_{i(n_x+2)}^x (Q_x)_{n_x l} \tag{35}$$
$$+D_{l(n_y+1)}^y (Q_y)_{i1} + D_{l(n_y+2)}^y (Q_y)_{in_y} = 0$$
$$(i = 2,3,\ldots,n_x - 1; l = 2,3,\ldots,n_y - 1)$$

$$\sum_{k=1}^{n_x} D_{ik}^x w_{kl} + 2\sum_{j=1}^{n_x}\sum_{k=1}^{n_y} B_{ij}^x B_{lk}^y w_{jk} + \sum_{k=1}^{n_y} D_{lk}^y w_{ik}$$
$$+D_{i(n_x+1)}^x (w_x)_{1l} + D_{i(n_x+2)}^x (w_x)_{n_x l}$$
$$+D_{l(n_y+1)}^y (w_y)_{i1} + D_{l(n_y+2)}^y (w_y)_{in_y} =$$
$$\frac{\sigma_\circ h}{D} \times \{\sum_{k=1}^{n_x} B_{ik}^x w_{kl} (\alpha_x)_{il} \tag{36}$$
$$+2\sum_{j=1}^{n_x}\sum_{k=1}^{n_y} A_{ij}^x A_{lk}^y w_{jk} (\alpha_{xy})_{il} + \sum_{k=1}^{n_y} B_{lk}^y w_{ik} (\alpha_y)_{il}\}$$
$$(i = 2,3,\ldots,n_x - 1; l = 2,3,\ldots,n_y - 1)$$

In these expressions, the symbols D_{ij}^x and D_{ij}^y denote the weighting coefficients corresponding to the fourth-order derivatives with respect to the x and y-directions, respectively. Similarly, B_{ij}^x and B_{ij}^y represent the weighting coefficients for second-order derivatives, while A_{ij}^x and A_{ij}^y correspond to the weighting coefficients for first-order derivatives. The terms Q_{ij} represent the values of the Airy stress function at the grid points.

$$\alpha_x = \frac{\sigma_x}{\sigma_\circ}, \alpha_{xy} = \frac{\tau_{xy}}{\sigma_\circ}, \alpha_y = \frac{\sigma_y}{\sigma_\circ} \tag{37}$$

As noted previously, the stress components cannot be obtained directly. Instead, they are derived through a matrix formulation:

$$[k_{ib} k_{ii}] \begin{Bmatrix} Q_b \\ Q_i \end{Bmatrix} = \{0\} \tag{38}$$

In this equation, the indices i and b correspond to internal and boundary grid points, respectively. By solving Eq. 35, the values of the Airy stress function Q_{ij} are obtained. Once these values are determined, the internal stress components can be calculated as follows:

$$(\sigma_x)_{il} = \sum_{k=1}^{n_y} B_{lk}^y Q_{ik}$$
$$(\tau_{xy})_{il} = -\sum_{j=1}^{n_x}\sum_{k=1}^{n_y} A_{ij}^x A_{lk}^y Q_{jk} \tag{39}$$
$$(\sigma_y)_{il} = \sum_{k=1}^{n_x} B_{lk}^x Q_{kl}$$
$$(i = 1,2,\ldots,n_x; l = 1,2,\ldots,n_y)$$

For each boundary point excluding the corner points along the edge *il* (where *i*=1 or $n_x; l = 2,3,\dots,n_y - 1$) parallel to the y-axis, the bending momentum $(M_x)_{ij}$ is expressed as:

$$(M_x)_{il} = -\frac{E_3}{1-\nu_\circ^2}\left(\sum_{k=1}^{n_x} B_{ik}^x w_{kl} + \nu \sum_{k=1}^{n_y} B_{lk}^y w_{ik}\right) \qquad (40)$$

Likewise, for each boundary point excluding the corner points along the edge *il* (where *l*=1 or $n_y; i = 2,3,\dots,n_x - 1$) parallel to the x-axis, the bending moment $(M_y)_{ij}$ is expressed as:

$$(M_y)_{il} = -\frac{E_3}{1-\nu_\circ^2}\left(\nu \sum_{k=1}^{n_x} B_{ik}^x w_{kl} + \sum_{k=1}^{n_y} B_{lk}^y w_{ik}\right) \qquad (41)$$

The primary objective of this study is to determine the buckling coefficient, which is defined as:

$$k = \frac{\sigma_\circ h b^2}{\pi^2 D} \qquad (42)$$

The value of $\sigma_\circ h/D$ to a specific eigenvalue obtained from Eq. 36 and is computed using numerical software packages such as Maple and MATLAB, as reported in the corresponding tables [41, 42]. To achieve faster convergence, the obtained $n_x = n_y = n$ is incorporated into the preceding calculation. In addition, the following relations are employed to compute the weighting coefficients:

$$x_i = -a\cos\left[\frac{(i-1)\pi}{n-1}\right]/2$$

$$y_i = -b\cos\left[\frac{(i-1)\pi}{n-1}\right]/2 \qquad (43)$$

$$i = 1,2,\dots,n$$

2.5. Specifications of the sample FGM plate

A rectangular plate made of a FGM composed of aluminum and alumina is considered in this study [43, 44]. The material properties of the constituent phases are defined as follows:

- Aluminum (Metal Constituent) $E_m = 70GPa$
- Alumina (Ceramic Constituent) $E_c = 380GPa$

3. Results and discussion

The fundamental limitations of Classical Plate Theory (CPT) in the analysis of plates fabricated from FGMs stem from the inherent incompatibility between the simplifying assumptions of the theory and the heterogeneous nature of material property variations. CPT assumes that lines normal to the mid-plane remain straight and perpendicular to the plane after deformation, thereby neglecting transverse shear deformation through the thickness. While this assumption is reasonable for homogeneous thin plates, it becomes increasingly inadequate for FGMs, in which shear stresses not only exist but may also exhibit nonlinear and asymmetric distributions due to the gradual and often pronounced variation of mechanical properties through the thickness. Moreover, CPT assumes the transverse normal stresses to be negligible. However, in FGM plates with moderate thickness-to-length ratios, these stresses particularly near boundaries or under localized loading can play a dominant role in initiating buckling or triggering material instability. The theory is also incapable of capturing critical phenomena such as virtual interlayer separation, which may arise from steep material gradients, or localized stress concentrations at specific depths within the plate. As a consequence, CPT-based predictions of critical buckling loads tend to be conservative for thicker FGM plates, as the softening effects associated with shear deformation are not accounted for. In summary, although CPT remains an efficient and reliable tool for the analysis of homogeneous thin plates, it lacks the necessary fidelity to accurately represent the mechanical response of modern FGM structures. In engineering applications where material gradients introduce significant mechanical complexity and sensitivity, uncritical application of CPT may lead to inaccurate predictions and potentially unsafe design outcomes. To determine the buckling coefficient, the first step involves computing the distribution of the Airy stress function using the MDQM. These stress components are subsequently substituted into the buckling equation, which has been reformulated within the DQ framework, in order to extract the corresponding buckling coefficient λ. By inserting the obtained value of λ into Eq. 42, the dimensionless buckling coefficient is calculated. The resulting system of equations is solved using Maple and MATLAB software packages. The buckling coefficient is evaluated for various grid densities under nonlinear compressive loading and different boundary conditions. By assigning a Power-Law Index value of zero, the FGM plate reduces to an equivalent homogeneous material, allowing direct comparison with benchmark solutions reported in the literature. After ensuring sufficient numerical accuracy and convergence, the buckling coefficients are computed for different values of the Power-Law Index corresponding to the FGM plate, and the results are presented in graphical and tabular form. As illustrated in Figure 4, the stress function distribution along the grid points (n=9) at the plate edges $x = \pm\frac{a}{2}$ is compared with the applied load. This comparison demonstrates the high effectiveness of the DQM in solving the present class of problems. Additional numerical results are presented in Figures 5 - 9 and Tables 1 - 5.

10.57647/Jsm.2025.1704.16

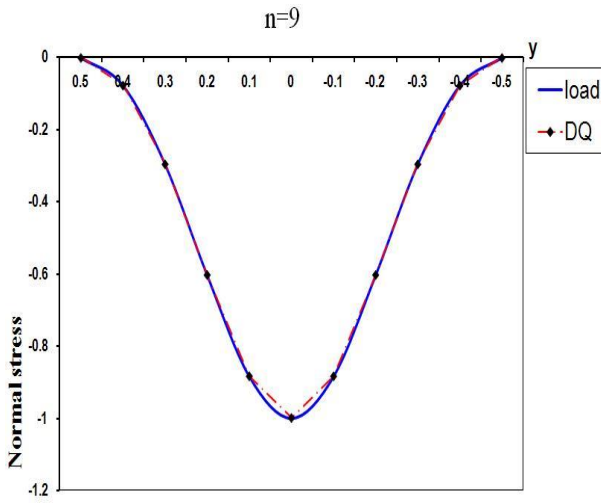

Figure 4. Normal stress distribution in $x = \pm\frac{a}{2}$ (n = 9)

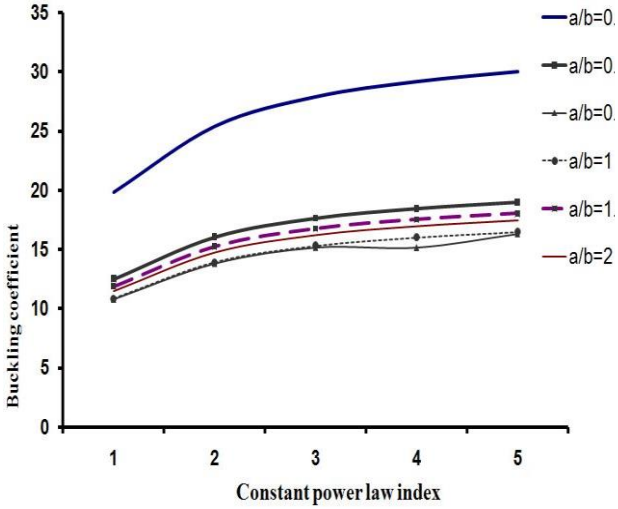

Figure 5. Buckling coefficient of the plate subjected to compressive $\sigma_x = -\sigma_0\, cos(\frac{\pi y}{b})$, under SSSS boundary conditions, for different values of the Power-Law Index (n = 11)

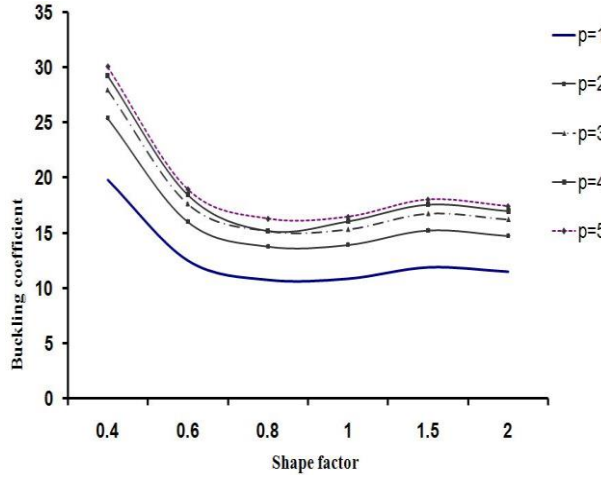

Figure 6. Buckling coefficient of the plate subjected to compressive$\sigma_x = -\sigma_0\, cos(\frac{\pi y}{b})$, under SSSS boundary conditions, for different values of the Power-Law Index (n = 11)

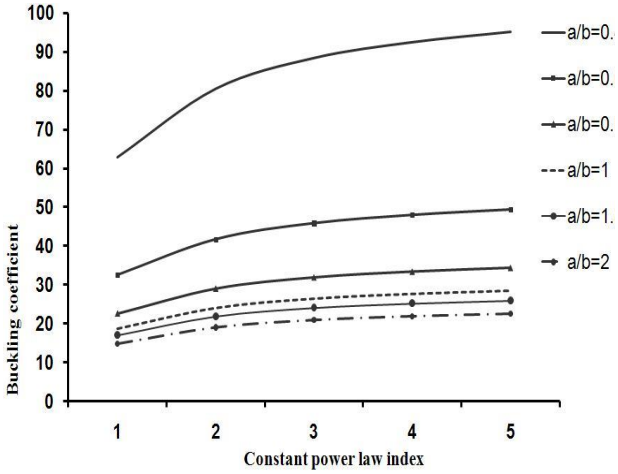

Figure 7. Buckling coefficient of the plate subjected to compressive $\sigma_x = -\sigma_0\, cos(\frac{\pi y}{b})$, under CSCS boundary conditions (n = 9)

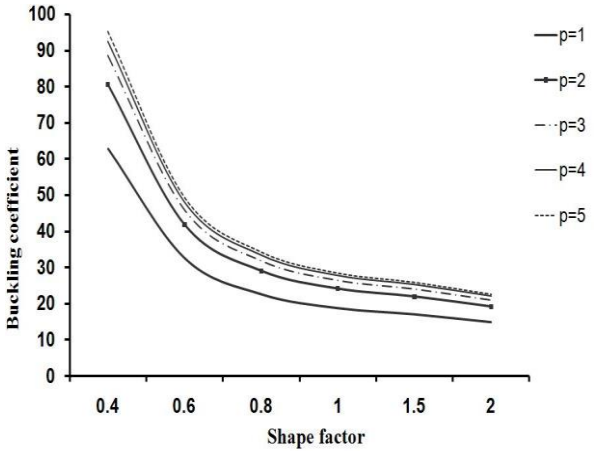

Figure 8. Buckling coefficient of the plate subjected to compressive $\sigma_x = -\sigma_0\, cos(\frac{\pi y}{b})$, under CSCS boundary conditions (n = 9)

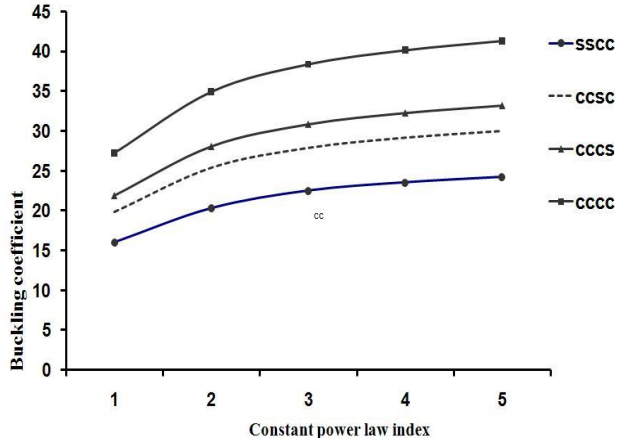

Figure 9. Buckling coefficient of the plate subjected to compressive $\sigma_x = -\sigma_0\, cos(\frac{\pi y}{b})$, under various boundary conditions for a shape factor of (a / b = 1)

10.57647/Jsm.2025.1704.16

Table 1. Buckling coefficient of the plate subjected to compressive$\sigma_x = -\sigma_0 \cos(\frac{\pi y}{b})$,under SSSS boundary conditions for different grid configurations

1.0	0.8	0.6	0.4		a/b
5.384	5.327	6.195	9.838		FEM
5.419	5.366	6.239	9.884	n= 9	
5.419	5.366	6.239	9.884	n=11	wang
5.419	5.366	6.239	9.884	n=13	
5.419	5.362	6.244	9.879	n= 9	
5.417	5.362	6.243	9.879	n=11	present
5.419	5.365	6.243	9.879	n=13	

Table 2. Buckling coefficient of the plate subjected to compressive $\sigma_x = -\sigma_0 \cos(\frac{\pi y}{b})$, under SSSS boundary conditions for different values of the power-law index (n = 11)

1.5	1.0	0.8	0.6	0.4	a/b
11.906	10.872	10.766	12.518	19.831	P=1
15.257	13.933	13.797	16.042	25.413	P=2
16.763	15.308	15.159	17.625	27.922	P=3
17.535	16.013	15.157	18.436	29.207	P=4
18.042	16.476	16.315	18.969	30.051	P=5

Table 3. Buckling coefficient of the plate subjected to compressive $\sigma_x = -\sigma_0 \cos(\frac{\pi y}{b})$, under SSSS boundary conditions for different grid densities (a / b = 0.4)

17	15	13	11	9	n
19.821	19.821	19.821	19.821	19.821	p=1
25.401	25.401	25.401	25.401	25.401	p=2
27.907	27.907	27.907	27.907	27.907	p=3
29.193	29.193	29.193	29.193	29.193	p=4
30.036	30.036	30.036	30.036	30.036	p=5

Table 4. Buckling coefficient of the plate subjected to compressive $\sigma_x = -\sigma_0 \cos(\frac{\pi y}{b})$, under SSSS boundary conditions (n = 9)

1.5	1.0	0.8	0.6	0.4	a/b
17.114	18.809	22.652	32.603	62.819	P=1
21.932	24.105	29.028	41.781	80.503	P=2
24.097	26.484	31.893	45.905	88.448	P=3
25.206	27.703	33.362	48.019	92.521	P=4
25.935	28.504	34.326	49.406	95.195	P=5

Table 5. Buckling coefficient of the plate subjected to compressive $\sigma_x = -\sigma_0 \cos(\frac{\pi y}{b})$, under different boundary conditions for a shape factor (a / b = 1)

p=5	p=4	p=3	p=2	p=1	p
24.235	23.554	22.517	20.295	15.993	SSCC
30.003	29.160	27.876	25.372	19.799	CCSC
33.171	32.239	30.820	28.051	21.889	CCCS
41.288	40.125	38.363	34.916	27.246	CCCC

To facilitate interpretation, the four plate edges are denoted as $x = -\frac{a}{2}, y = -\frac{b}{2}, x = \frac{a}{2}, y = \frac{b}{2}$. For instance, the CSCS boundary condition indicates that the plate edges along $x = \pm\frac{a}{2}$ are simply supported, while the remaining edges ($y = \pm\frac{b}{2}$) are clamped. Initially, rectangular plates with different parameter values under SSSS boundary conditions are analyzed. As reported in Table 1, the buckling coefficients are computed for various grid densities and subsequently compared with the results reported by Wang as well as corresponding finite element solutions. The plate is subjected to cosine compressive loading. The results obtained using the DQM exhibit close agreement with the finite element solutions, and the convergence behavior of the MDQM is notably rapid, confirming the accuracy and reliability of the proposed method. In Table 2, the buckling coefficient under identical compressive loading is examined for simply supported boundary conditions with a fixed number of grid points (n=11). In this case, both σ_x and$\sigma_y$are zero, whereas $\tau \neq 0$is nonzero. As shown in Figure 2, the value of τ_{xy} remains nonzero along the plate edges $y = \pm\frac{b}{2}$. Moreover, the shear stress components along these two edges exhibit opposite signs. As the number of grid points increases, the shear stress (τ_{xy}) component approaches zero, and the MDQM results increasingly converge toward the finite element data. Table 2 further demonstrates that the buckling coefficient increases with increasing Power-Law Index, whereas an increase in the aspect ratio (a/b) leads to a reduction in the buckling coefficient, as also illustrated in Figures 5 and 6. According to the results presented in Table 3, the buckling coefficient remains nearly unchanged across different grid densities, particularly when a sufficiently large number of grid points is employed. The results reported in Table 4 follow a similar trend to those in Table 2; however, the buckling coefficient varies depending on the boundary conditions applied. Table 5 presents the buckling coefficients corresponding to different boundary conditions for an aspect ratio of (a/b=1), with the associated trends illustrated in Figure 9. As observed, variations in boundary conditions significantly influence the buckling response, and an increase in the number of clamped edges leads to higher buckling coefficients. Overall, the buckling coefficient is strongly dependent on

10.57647/Jsm.2025.1704.16

the imposed boundary conditions. The close agreement between the MDQM predictions and finite element results confirms that the MDQM is a robust and accurate approach for determining the buckling loads of plates subjected to non-uniform in-plane loading.

4. Conclusion

This study demonstrated that the Modified Differential Quadrature Method (MDQM), combined with integrated boundary conditions, is an efficient and reliable numerical tool for analyzing the buckling behavior of rectangular plates made of FGMs. By transforming the governing differential equations into a system of linear algebraic equations, critical buckling loads were accurately computed. The close agreement between the MDQM results and those obtained from finite element analysis confirms the validity and accuracy of the proposed approach. In this work, the MDQM was employed to investigate the buckling response of thin rectangular plates subjected to parabolic in-plane compressive loading. Two types of boundary conditions simply supported and clamped edges were considered. The buckling analysis was performed in two main stages: (1) Calculation of the in-plane stress distribution, and (2) solution of the buckling problem using the stress fields obtained in the first stage. The results indicate that solutions to the in-plane elasticity problem obtained using the DQM are highly sensitive to the number of grid points. When an insufficient number of grid points is used, the results fail to converge, highlighting the importance of appropriate grid selection for the effective application of the MDQM. Furthermore, the numerical results demonstrate that changing the boundary conditions from simply supported to clamped leads to an increase in the buckling coefficient. It was also observed that increasing the exponent in the FGM material property distribution law results in higher critical buckling loads due to the associated increase in plate stiffness. By employing the Airy stress function together with integrated boundary conditions, a practical and effective approach for computing pre-buckling stresses under non-uniform loading conditions was achieved. The proposed framework showed strong performance for variable load distributions, such as cosine-type loading.

Overall, this study highlights the capability of the MDQM in addressing engineering problems involving complex boundary conditions and non-homogeneous material behavior. With further extension to incorporate higher-order deformation theories and broader classes of loading and geometries, the MDQM can serve as a powerful and efficient numerical framework for the analysis and design of advanced heterogeneous structures in modern industrial applications.

Authors Contribution
Reza Kazemi raised the topic of this research, studied it to obtain the required results and data, and analyzed them.
Mohsen Rafiei Karahroudi collected the data and conducted some aspects of this research work.
Seyed Alireza Mousavi Shirazi authored the manuscript, arranged all its parts, and responded to and answered the reviewers' comments.

Availability of data and materials
The data that support the findings of this study are available from the corresponding author, upon reasonable request.

Conflict of interests
The author states that there is no conflict of interest.

References

[1] Das, S., and Jana, P. 2024, Rigorous plane-stress solution and buckling analysis of rectangular functionally graded plates subjected to non-uniform edge loads, *Mechanics Based Design of Structures and Machines* 52(5):2775-2803. https://doi.org/10.1080/15397734.2023.2190823

[2] Mittelstedt, C. 2023, Theory of plates and shells. Berlin, Heidelberg: Springer Vieweg.

[3] Mamandi, A., 2023, Finite element based bending analysis of rectangular FGM plates using first-order shear deformation theory, *Journal of Mechanical Science and Technology* 37(5):2491-2506. https://doi.org/10.1007/s12206-023-0425-6

[4] Duran, A.V., et al. 2015, Thermal buckling of composite plates with spatial varying fiber orientations, *Composite Structures* 124:228-235. https://doi.org/10.1016/j.compstruct.2014.12.065

[5] Mossavarali, A., and Eslami, M.R. 2002, Thermoelastic buckling of plates with imperfections based on a higher order displacement field, *Journal of thermal stresses* 25(8):745-771. https://doi.org/10.1080/01495730290074513

[6] Fox, L. 2012, Numerical solution of ordinary differential equations. Springer Science & Business Media.

[7] Benounas, S., et al. 2025, Improved first-order shear deformation-based finite element approach for predicting free vibration frequencies of functionally graded sandwich doubly curved shallow shells, *Journal of Engineering Mathematics* 152(1):8. https://doi.org/10.1007/s10665-025-10448-5

[8] Xing, Y., et al. 2010, A differential quadrature finite element method, *International Journal of Applied Mechanics* 2(01):207-227. https://doi.org/10.1142/S1758825110000470

[9] Bhullar, S.K., and Wegner, J.L. 2009, Some transient thermoelastic plate problems, *Journal of Thermal Stresses* 32(8):768-790. https://doi.org/10.1080/01495730903018499

[10] Saini, R. 2025, Vibration Analysis of Bi-Directional Heated Functionally Graded Circular Nanoplates With Variable Thickness Using Generalized Differential Quadrature Method Integrated With Parallel Computing, *International Journal of Structural Stability and Dynamics* 2650214. https://doi.org/10.1142/S0219455426502147

[11] Fereidoon, A., et al. 2011, Bending analysis of thin functionally graded plates using generalized differential quadrature method, *Archive of Applied Mechanics* 81(11):1523-1539. https://doi.org/10.1007/s00419-010-0499-3

[12] Shirazi, S.A.M. 2012, March. The assessment of radioisotopes and radiomedicines in the MNSR reactor of Isfahan and obtaining the burnup by applying the obtained information, In 2012 *Asia-Pacific Power and Energy Engineering Conference* (pp. 1-4). IEEE, https://doi.org/10.1109/APPEEC.2012.6307050

[13] Torabi, J., et al. 2020, Mechanical buckling analyses of sandwich annular plates with functionally graded carbon nanotube-reinforced composite face sheets resting on elastic foundation based on the higher-order shear deformation plate theory, *Journal of Sandwich Structures & Materials* 22(6):1812-1813. https://doi.org/10.1177/1099636218789617

[14] B Bhagat, V., and Jeyaraj, P. 2018, Experimental investigation on buckling strength of cylindrical panel: effect of non-uniform temperature field, *International Journal of Non-Linear Mechanics* 99:247-257. https://doi.org/10.1016/j.ijnonlinmec.2017.12.005

[15] Benoy, M.B. 1969, An energy solution to the buckling of rectangular plates under non-uniform in-plane loading, *The Aeronautical Journal* 73(707):974-977. https://doi.org/10.1017/S0001924000051423

[16] Wang, X., and Yuan, Z. 2018, Buckling analysis of isotropic skew plates under general in-plane loads by the modified differential quadrature method, *Applied Mathematical Modelling* 56:83-95. https://doi.org/10.1016/S0263-8231(02)00100-3

[17] Numayr, K.S., et al. 2024, Approximate solutions for bending of beams and buckling of columns made of functionally graded materials, *Journal of The Institution of Engineers (India): Series A* 105(4):913-937. https://doi.org/10.1007/s40030-024-00834-0

[18] Ahlawat, N., and Saini, R. 2024, Vibration and buckling analysis of elastically supported bi-directional FGM mindlin circular plates having variable thickness, *Journal of Vibration Engineering & Technologies* 12(1):513-532. https://doi.org/10.1007/s42417-023-00856-1

[19] Kumar, R., et al. 2023, Geometrically nonlinear analysis for flexure response of FGM plate under patch load, *Mechanics Based Design of Structures and Machines* 51(11):6532-6556. https://doi.org/10.1080/15397734.2022.2058015

[20] Khalid, H.M., et al. 2022, Inverse differential quadrature method for structural analysis of composite plates, *Computers & Structures* 263:106745. https://doi.org/10.1016/j.compstruc.2022.106745

[21] Mousavi Shirazi, S.A. 2015, Numerical solution of diffusion equation to study fast neutrons flux distribution for variant radii of nuclear fuel pin and moderator regions, *Kerntechnik* 80(3):291-294. https://doi.org/10.3139/124.110498

[22] Javani, M., et al. 2021, Rapid heating vibrations of FGM annular sector plates, *Engineering with Computers* 37(1):305-322. https://doi.org/10.1007/s00366-019-00825-x

[23] Tang, Y.Q., et al. 2024. Modified differential quadrature method using basis functions satisfying multiple boundary conditions for buckling analyses of beams and rectangular plates. *Journal of Engineering Mechanics* 150(8):04024054. https://doi.org/10.1061/JENMDT.EMENG-773

[24] Wang, X., et al. 2014, Accurate vibration analysis of skew plates by the new version of the differential quadrature method, *Applied Mathematical Modelling* 38(3):926-937. https://doi.org/10.1016/j.apm.2013.07.021

[25] Kumar, R., et al. 2024, Initial buckling behavior of elastically supported rectangular FGM plate based on higher order shear deformation theory via spline RBF method, *Mechanics of Advanced Composite Structures* 11(1):59-72. https://doi.org/10.22075/macs.2023.30125.1484

[26] Civalek, Ö., and Avcar, M. 2022, Free vibration and buckling analyses of CNT reinforced laminated non-rectangular plates by discrete singular convolution method, *Engineering with Computers* 38(Suppl 1):489-521. https://doi.org/10.1007/s00366-020-01168-

[27] Allahkarami, F. 2022, Dynamic buckling of functionally graded multilayer graphene nanocomposite annular plate under different boundary conditions in thermal environment, *Engineering with Computers* 38(Suppl 1):583-606. https://doi.org/10.1007/s00366-020-01169-7

[28] Meksi, R., et al. 2019, An analytical solution for bending, buckling and vibration responses of FGM sandwich plates, *Journal of Sandwich Structures & Materials* 21(2):727-757. https://doi.org/10.1177/1099636217698443

[29] Wang, X., et al. 2007, Accurate buckling loads of thin rectangular plates under parabolic edge compressions by the differential quadrature method, *International Journal of Mechanical Sciences* 49:447-453. https://doi.org/10.1016/j.ijmecsci.2006.09.004

[30] Wu, C.P., and Liu, Y.C. 2016, A state space meshless method for the 3D analysis of FGM axisymmetric circular plates, *Steel and Composite Structures* 79:528-531. https://doi.org/10.12989/scs.2016.22.1.161

[31] Karahroudi, M.R., and Mousavi Shirazi, S.A. 2014, Obtaining the neutronic and thermal hydraulic parameters of the VVER-1000 Bushehr nuclear reactor core by coupling nuclear codes, *Kerntechnik* 79:528-531. https://doi.org/10.3139/124.110440

[32] Mohammadi, M., et al. 2021, Functionally graded materials (FGMs): A review of classifications, fabrication methods and their applications, *Processing and Application of Ceramics* 15(4):319-343. https://doi.org/10.2298/PAC2104319M

[33] Belabed, Z., et al. 2014, An efficient and simple higher order shear and normal deformation theory for functionally graded material (FGM) plates, *Composites Part B: Engineering* 60:274-283. https://doi.org/10.1016/j.compositesb.2013.12.057

[34] Wang, X., et al. 2003, Buckling analyses of anisotropic plates and isotropic skew plates by the new version differential quadrature method, *Thin-Walled Structures* 41(1):15-29. https://doi.org/10.1016/S0263-8231(02)00100-3

[35] Bhaskar, K., and Varadan, T.K. 2021, Classical plate theory. In Plates: *Theories and Applications, Springer* 11-28. https://doi.org/10.1007/978-3-030-69424-1

[36] Ike, C.C. 2019, Solution of elasticity problems in two dimensional polar coordinates using Mellin transform, *Journal of Computational Applied Mechanics* 50(1):174-181. https://doi.org/10.22059/jcamech.2019.278288.370

[37] Guzev, M.A. 2021, February. The Airy Stress Function for Non-Euclidean Model of a Continuous Medium and Description of Residual Stresses. In Smart Modelling For Engineering Systems: *Proceedings of the International Conference on Computational Methods in Continuum Mechanics (CMCM 2021) (pp. 75-85). Singapore: Springer* 75-85. https://doi.org/10.1007/978-981-33-4709-0_7

[38] Barber, J.R. 2023, Elasticity. London New York, Heidelberg: Springer Dordrecht.

[39] Karimi Pour, A., and Noroozinejad Farsangi, E. 2023, Airy stress function for proposed thermoelastic triangular elements, *Journal of Engineering Mathematics* 138(1):11. https://doi.org/10.1007/s10665-022-10256-1

[40] Huo, R., et al. 2023, Transverse vibration and buckling analysis of rectangular plate under arbitrary in-plane loads, *Acta Mechanica* 234(9):3917-3931. https://doi.org/10.1115/1.802946.paper26

[41] Wang, X., et al. 2005, New approaches in application of differential quadrature method to fourth-order differential equations, *Communications in Numerical Methods in Engineering* 21(2):61-71. https://doi.org/10.1002/cnm.727

[42] Taj, M.G., and Chakrabarti, A. 2013, Buckling analysis of functionally graded skew plates: An efficient finite element approach, *International Journal of Applied Mechanics* 5(04):1350041. https://doi.org/10.1142/S1758825113500415

[43] Mousavi Shirazi, S.A., and Rastayesh, S. 2011, The comparative investigation and calculation of thermo-neutronic parameters on two gens II and III nuclear reactors with same powers, *fuel* 100:60. https://doi.org/10.5281/zenodo.1329156

[44] Sadgui, A., and Tati, A. 2022, A novel trigonometric shear deformation theory for the buckling and free vibration analysis of functionally graded plates, *Mechanics of Advanced Materials and Structures* 29(27):6648-6663. https://doi.org/10.1080/15376494.2021.1983679